Free-standing films of twist grain boundary TGB$_A$ and UTGB$_{C*}$ liquid crystals studied by fluorescence confocal polarizing microscopy

I. I. SMALYUKH, R. PRATIBHA†, O. D. LAVRENTOVICH* and
N. V. MADHUSUDANA†

Chemical Physics Interdisciplinary Program and Liquid Crystal Institute,
Kent State University, PO Box 5190, Kent, OH 44242-0001, USA
†Raman Research Institute, C. V. Raman Avenue, Bangalore 560 080, India

The director structures, meniscus profile, and defects in free-standing films of the twist grain boundary TGB$_A$ and UTGB$_{C*}$ liquid crystals were studied. The films were characterized by a combination of polarizing microscopy and fluorescence confocal polarizing microscopy. Five principal regions of meniscus were distinguished. When film thickness in the meniscus is much smaller then the TGB pitch, there is no difference between the free-standing films of TGB and ordinary smectic A liquid crystals. When the film thickness is larger than the TGB pitch, filamentary texture is observed. The 3D director pattern of the filaments are similar to the ground state director fields of TGB$_A$ and UTGB$_{C*}$ liquid crystals. In the intermediate thickness region of the meniscus, when the film thickness and TGB pitch are commensurate, a unique radial pattern is observed. Based on the fluorescence confocal polarizing microscopy studies of the director field, we propose a model for the 3D director structure in this part of the meniscus.

1. Introduction

The similarities between the nematic (N) – smectic A (SmA) transition in liquid crystals (LCs) and the normal metal – superconductor phase transition were first recognized by de Gennes [1]. He predicted the possibility of an intermediate phase with a regular defect structure. Renn and Lubensky extended this to chiral systems and pointed out that the intrinsic twist of the cholesteric phase can act as an external field. They described the structure of the twist grain boundary TGB$_A$ phase as having blocks of smectic A liquid crystal regularly stacked in a helical fashion along an axis parallel to the smectic layers [2]. The slabs are separated by an array of screw dislocations. The prediction of the TGB$_A$ phase was substantiated by the experimental observations of Goodby *et al.* [3] and others [4, 5]. Other types of TGB phases, such as the TGB$_C$ and TGB$_{C*}$ phases have been described theoretically [6, 7] and the TGB$_C$ phase has also been experimentally characterized [8]. Recently, a new type of TGB phase, called the undulating twist grain boundary C* (UTGB$_{C*}$) phase, has been experimentally found in binary mixtures of a chiral and a non-

chiral compound [9] and later theoretically explained in [10]. This liquid crystal phase is characterized by a two-dimensional undulation of the smectic blocks and the grain boundaries in the form of a square lattice normal to the TGB helix. Since even the ground state of this new type of grain boundary phase is characterized by complex molecular arrangements, one may expect observation of interesting director structures under different conditions of confinement, anchoring and in the vicinity of phase transitions.

Polarizing microscopy (PM) of free-standing films is a powerful tool in the study of LC phases [11]. This method is useful in studies of smectic phases in which the film thickness can be as small as a few smectic layers in the flat part of the film. Recently, attention has been drawn to the meniscus region of free-standing SmA films [12], in which the film thickness usually changes over a large range from tens of nanometers to tens of microns. The meniscus part of a free-standing SmA film was later described as composed of distinct regions [13]. New types of defects observed in free-standing films have been used to identify the TGB$_A$ phase [14, 15]. More recently observations on the meniscus region of free-standing films of the TGB$_A$ and UTGB$_{C*}$ phases, using transmission polarizing microscopy, have been made [16]. A rich variety of textures

*Author for correspondence; e-mail: odl@lci.kent.edu

has been reported. In this paper we describe detailed systematic studies carried out on the same system using fluorescence confocal polarizing microscopy (FCPM) [17, 18].

In this work we have studied free-standing films of a LC mixture of a chiral and a non-chiral compound exhibiting both the TGB$_A$ and UTGB$_{C*}$ phases. A whole variety of complex 3D director structures was observed and characterized. We show distinct and similar features of director patterns in the two different grain boundary phases. We also describe a new and rather unusual type of director structure present in the intermediate thickness region of the meniscus, with stripes extending radially. To study the complex director structures and to characterize the meniscus profile, we have employed the recently developed technique of FCPM [17, 18] which allows for 3D resolution in studies of LC structures.

2. Experimental
2.1. Materials

The chiral compound used in the binary mixture was (4-2′-methylbutyl)phenyl 4′-*n*-octylbiphenyl-4-carboxylate, exhibiting the phase sequence Cr 67 SmI* 70 SmC* 85 SmA 134.6 N* 140.5 I (temperatures in °C). The non-chiral compound was 2-cyano-4-heptylphenyl 4′-pentyl-4-biphenylcarboxylate, which exhibits only the nematic phase (Cr 45 N 102 I). It has been shown by X-ray studies that the latter has a strong skew cybotactic (SmC-like) short range order [19]. The particular mixture used in our study has the chiral and non-chiral compounds in the ratio of 64:36 by weight, respectively. The phase transitions exhibited by this mixture on cooling from the isotropic phase are:

I 121.7 BP$_1$ 121.5 BP$_2$ 121.2 N* 76.8 TGB$_A$ 63 UTGB$_{C*}$ 59 SmC* 45 Cr.

For FCPM studies, the specimen was doped with a high quantum-yield fluorescent dye. We used a very small amount (0.01 wt %, well below the solubility limit for both of the components of the LC mixture) of fluorescent dye N,N′-bis(2,5-di-tert-butylphenyl)-3,4,9,10-perylenedicarboximide (BTBP), purchased from Molecular Probes [17, 18]. The dye molecules are well oriented by the LC host. For BTBP dye, the fluorescence lifetime 3.7–3.9 ns is smaller than the characteristic time of rotational diffusion of liquid crystals (about 10 ns), and dye orientations during absorption and emission can be assumed to be close to each other. At the concentration used, the dye has no significant effect on the temperatures of phase transitions or on orientational order in the LC, but gives a sufficiently strong fluorescence signal for the FCPM studies. No strong photo-bleaching was observed in the samples studied. Since the thickness of the free standing

films was rather small, the 3D director structures could be studied despite the fact that the LC mixture has a rather large optical birefringence.

2.2. Experimental set-up

The principal scheme of the 2-channel confocal microscope used in the experiment is shown in figure 1. The microscope can work in the confocal fluorescence reflection and/or wide field transmission modes. The use of polarizers permits fluorescent confocal polarizing microscopy (FCPM) [17] and ordinary polarizing microscopy (PM). The interference filters allow for the spectral separation of light and thus simultaneous modes/channels of observation.

The region of the specimen inspected by FCPM is a small (submicron) voxel ($=$ 3D pixel), a diffraction-limited spot produced by a focused laser beam. Signals from nearby voxels are suppressed by a pinhole in the image space. A 40x air objective with $(NA) = 0.6$ was used, the pinhole diameter being set at 100 μm. The point source of light, the inspected voxel, and the pinhole are confocal. Fluorescence light from the voxel (focal plane) passes through the pinhole aperture located in the focal plane that is conjugate to the illuminated point of the specimen. Light coming from the neighbourhood of the inspected voxel is blocked from reaching the detector. To obtain the 3D image of the whole sample, the tightly focused laser beam scans the specimen voxel by voxel. It is implemented by optical scanning in the horizontal plane, followed by mechanical refocusing at a different depth in the sample and repeating the horizontal scanning. As a result, the image is presented as a stack of thin (submicron) horizontal optical slices. Using a computer, the data, containing an essentially 3D pattern, can be presented as horizontal or vertical 'cross-sections' of the sample.

Compared with the well known fluorescence confocal microscopy (FCM), FCPM has two distinctive features: (a) the specimen is stained with anisometric dye molecules (in this case, BTBP) that follow the director orientation; (b) the excitation light is polarized, usually linearly [17, 18]. The FCPM signal, resulting from a sequence of absorptions and emissions, strongly depends on the angle between the transition dipole of the dye molecules (parallel to the local director $\hat{\mathbf{n}}$) and polarizer **P**. The intensity of fluorescence is maximum when **P**$\|\hat{\mathbf{n}}$ and minimum when **P**$\perp\hat{\mathbf{n}}$. The strong orientation dependence of the measured fluorescence signal allows one to decipher the 3D orientation pattern from the FCPM observations.

The normal PM image is recorded by measuring the intensity of light that passes through the polarizer (**P**), the free standing LC film, and analyzer (**A**), as shown in
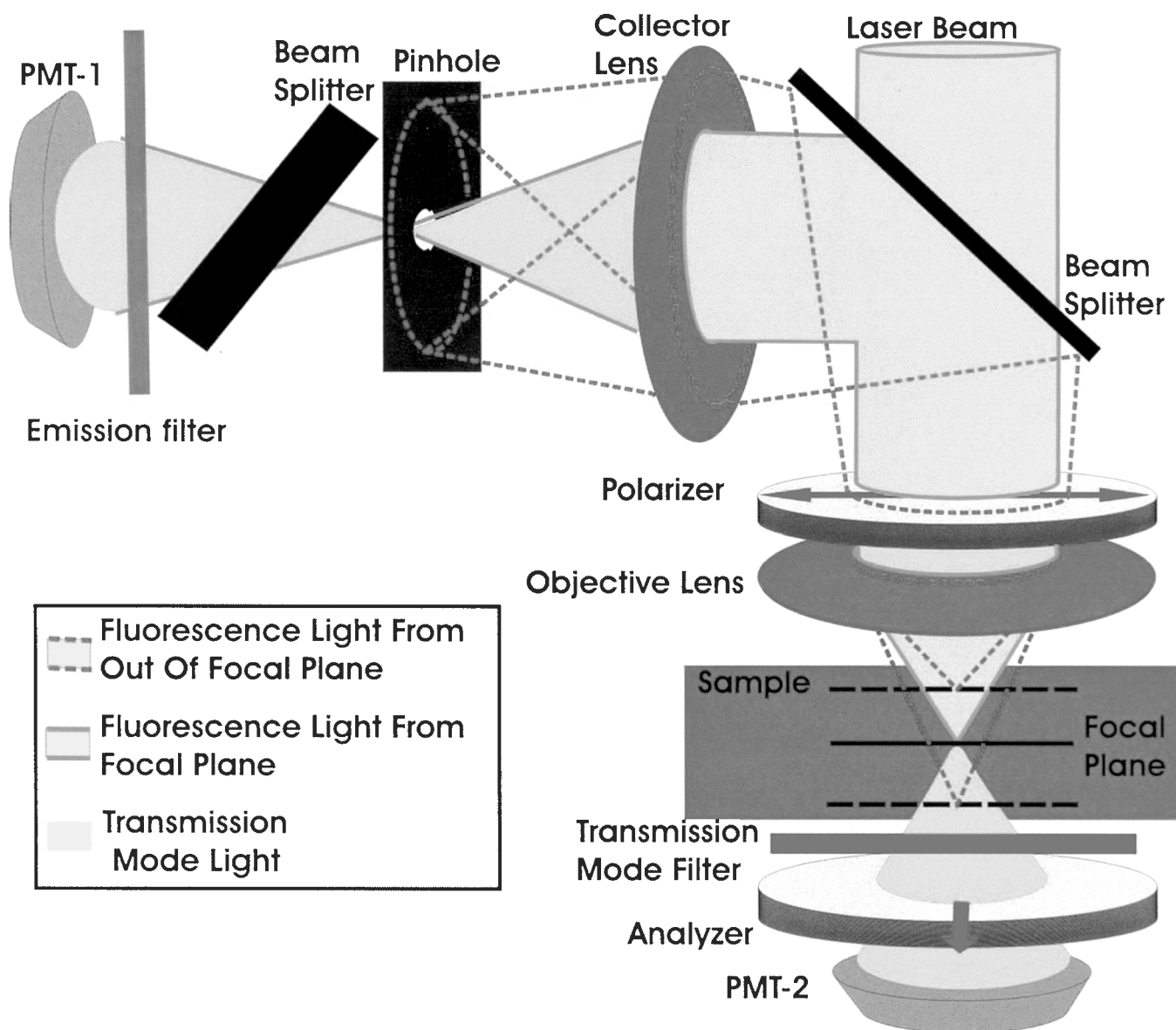
Figure 1. Experimental set-up used for fluorescence confocal polarising microscopy.

figure 1. To study the profile of the meniscus of the free standing films using the interference fringe pattern, we employed transmission mode wide field microscopy with the monochromatic light source being an Ar laser (488 nm, power less than 1 μW). The same laser was used as an excitation source for the FCPM studies. For the usual polarizing microscopy we used an achromatic light source, viz. a mercury lamp.

The fluorescent light from the doped liquid crystal film is detected by a photomultiplier tube (PMT-1) in the spectral region 510–550 nm as selected by interference filters (channel 1). The transmission mode light is detected by PMT-2 in the spectral region with $\lambda > 550$ nm (channel 2). The use of two detection channels permits simultaneous work in PM and FCPM modes and co-localization of the features of PM and FCPM textures.

2.3. *Free-standing films and their characterization*

The free-standing films were suspended across 2 mm wide holes drilled in either glass or metal plates. Before the FCPM and PM studies, the samples were maintained for several hours in order to obtain stationary film profiles and director structures. Additionally, after each change of temperature, the sample was equilibrated at the required temperature. The temperature was controlled using an MK1 hot stage with an accuracy of the order of 0.1 K.

In the region of interest the thickness of the free-standing film varies from the size of several smectic layers in its flat part to tens of microns. In the thinner part, where the film thickness is in the sub-micron and micron ranges, it is experimentally measured using the pattern of interference fringes. In the thicker part of the film, where the thickness ranges from microns to tens of microns, it is directly measured using the vertical FCPM cross-sections. The accuracy of the thickness measurements in the thicker part of the meniscus is determined by the axial resolution of the confocal microscope. The axial resolution for a sample of isotropic liquid would be $\Delta z_{iso} = 1.5 n \lambda / NA^2 \approx 2 \, \mu m$, where n is the average LC refractive index, and NA is the numerical aperture of the objective used. The axial resolution in our studies of films of highly anisotropic LC is somewhat worse due to the defocusing effects in the liquid crystal material, a birefringent medium [17, 18]. A rough estimate of the additional resolution worsening in a birefringent medium gives $\Delta z_{LC} \sim \Delta n Z / n$, where Z is the depth of scanning and Δn is the birefringence [17, 18]. In the FCPM vertical cross-sections, when the film thickness reaches tens of microns its profile becomes somewhat asymmetric due to different resolution at the top and bottom interfaces of the film (the bottom interface is blurred over $\Delta z \sim \Delta z_{iso} + \Delta n Z / n$, much stronger than the top interface where $Z = 0$). Therefore, we use the top LC–air interface of the vertical FCPM cross-sections (at which $Z = 0$ and the axial resolution Δz is not worse than $2.5 \, \mu m$) to analyse the thickness profile of the free

standing films. The accuracy of thickness measurements based on the interference fringes is much better ($\Delta z < 1 \, \mu m$). The film thickness data obtained by these two different methods are then extrapolated over the entire range of thickness of the meniscus.

All in-plane characteristic dimensions of director structures (such as periodicity of the radial structures, wavelength of undulations of filaments) in the free-standing film are measured using both PM and FCPM modes. The accuracy is mainly limited by the radial resolution of the microscope, and is about $1 \, \mu m$ in both cases.

3. Results

3.1. *Observation of different regions of the meniscus*

Figure 2 shows the general features of PM textures of free-standing films in the TGB phases. The central part of the film appeared completely dark between crossed polarizers. This indicates that the structure is unwound in the flat part of the film and that the smectic liquid crystal is homeotropic. On proceeding from the centre of the hole towards the supporting walls, several different regions of meniscus can be distinguished (in figures 2–9 these regions are marked by numbers 1–5). Another important observation is that the appearance of the textures in some parts of the film changes at the phase transition from TGB_A to $UTGB_{C*}$ phase, compare region 4 in figures 2(*a*) and 2(*b*); whereas in other parts the texture is unaltered, regions 1–3 in figures 2(*a*) and 2(*b*). The variety of observed PM textures is richer than in the case of the meniscus region
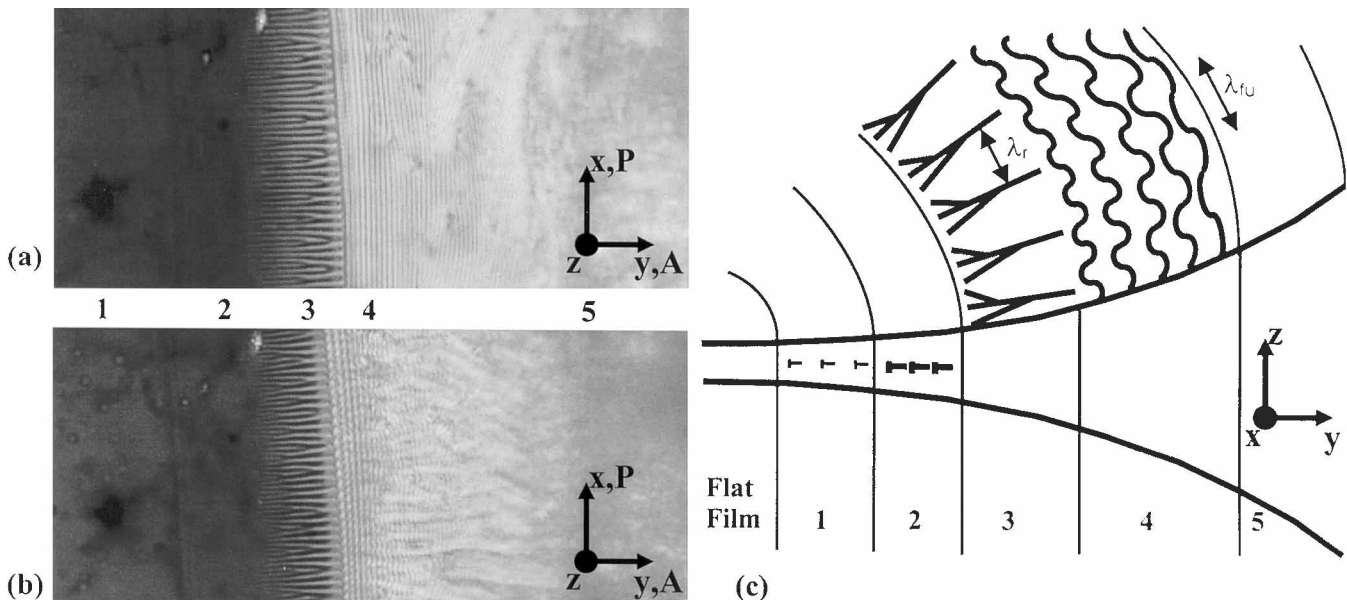
Figure 2. Meniscus region of the free standing film: polarizing microscopy textures of the LC mixture (*a*) in the TGB_A phase, and (*b*) in the $UTGB_C^*$ phase; (*c*) schematic representation of different regions of meniscus and corresponding structures.

of SmA films, described in [12]. In figure 2(c) we show a generalized representation of all the observed textures in different regions of the meniscus. λ_{fu} denotes the undulation wavelength of the filaments which is finite in the UTGB$_{C*}$ and becomes infinite in the TGB$_A$ phase.

The profile of the meniscus was determined using a combination of both PM and FCPM as described earlier. The interference fringes observed in the thinner part of the meniscus with d < 1 μm, figure 3(a), were used to measure the relative increase of the thickness in this region. Beyond this region, when d > 1 μm, FCPM was used to measure the film thickness from the vertical cross-sections of the free standing film, figure 3(b).

The region 1 is close to the central flat part of the film. In this region, the film thickness changes from several to hundreds of nanometers. The increase in thickness is accomplished by well separated dislocations of a small Burger's vector as seen in figure 4. Region 1 is completely analogous to a similar region in SmA films. The distortions in the film due to the dislocations are small and very difficult to visualize between crossed polarizers. Therefore, it is difficult to distinguish this region of the meniscus from the flat part of the film based only on PM textures. However, the dislocations of the small Burger's vector are clearly visualized by

means of transmission mode wide field microscopy using a monochromatic light source (figure 4). The distances between the dislocations are much larger than the film thickness. Thus, these dislocations can be considered as isolated and not interacting with each other (similar to the case of a Grandjean–Cano wedge with a small dihedron angle). Since the surface tension at the LC–air interface (about 30 dyn cm^{-1} [12]) is much larger than $\sqrt{K_{11}B}$, where K_{11} is the splay elastic constant and B is the Young's (or layer compressibility) modulus, it is expected that the interfaces repel the dislocations and they are found in the film mid-plane [20, 21].

The change of thickness in region 2 of the meniscus is accomplished via dislocations of relatively large Burger's vectors. In this region, the thickness is comparable to the wavelength of light and can be characterized by an analysis of the interference fringes. The film thickness increases from hundreds of nanometers to about a micron. The dislocations in this region cannot be considered as isolated. The equilibrium positions and Burger's vectors of these dislocations are determined by bulk elasticity and surface energy along with the varying film thickness. The profile of the film in this region is smooth, which can be understood, taking
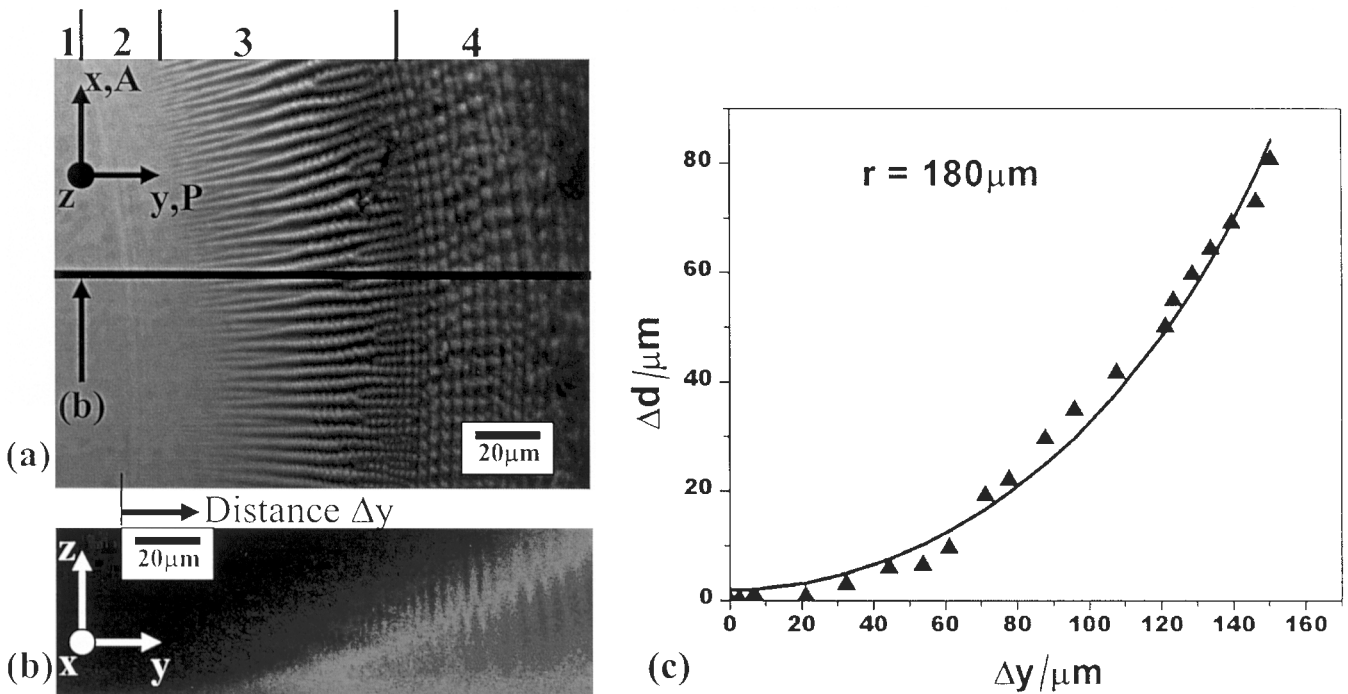
Figure 3. Meniscus region of the free-standing film as observed (a) with transmission mode polarizing microscopy, and (b) its vertical cross-section obtained with FCPM along the line in (a); relative increase Δd of the film thickness versus distance Δy measured along the line in (a). Solid line in (c) shows the best fit of a circular profile to the experimental data on thickness of the meniscus as a function of radial position obtained from the pattern of interference fringes in (a) and FCPM vertical section in (b).
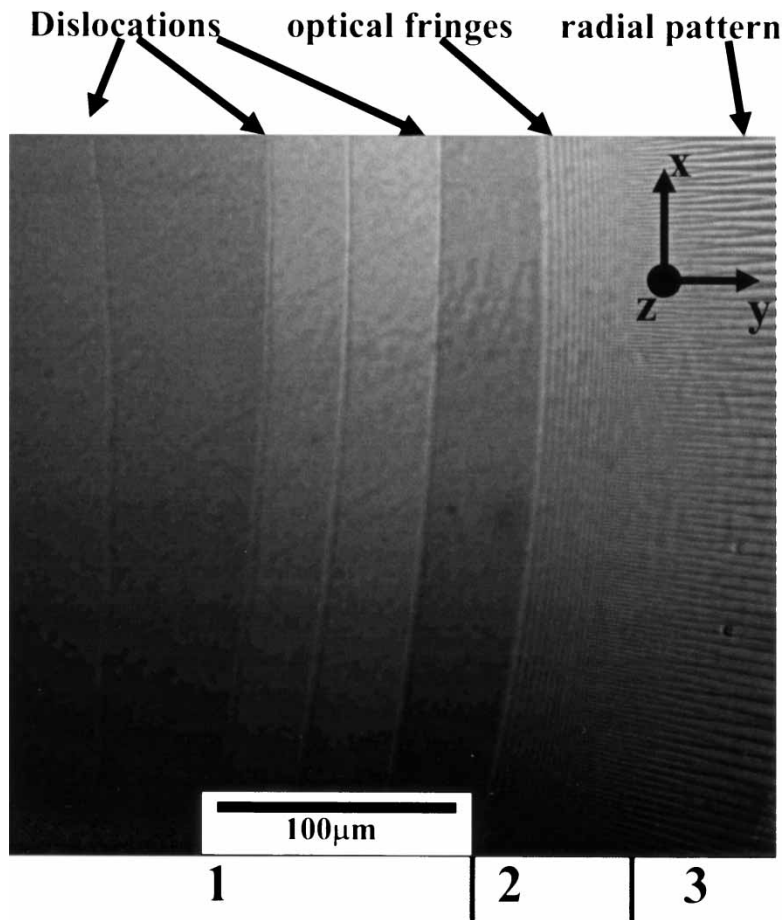
Figure 4.   Isolated dislocations in the region of meniscus corresponding to region 2 in figure 2, visualized using wide field optical microscopy and a monochromatic source of light ($\lambda = 488$ nm).

into account the large surface tension at the LC–air interface. Again, this region of the meniscus is analogous to a similar region in SmA films described in [12, 13], showing that in this thickness range the TGB phases behave similarly to ordinary SmA.

The second region of the meniscus smoothly transforms to the region 3 with radial structures, i.e. alternate bright and dark stripes, extending radially towards the centre of the film (figure 2). This texture is rather unusual for free standing films. Meyer and Pershan [22] have observed regularly spaced domains with similar appearance in free-standing SmC films, and explained them as due to surface polarization and periodic splay deformation of the *C*-director. In this case a rotation of the sample between crossed polarizers should result in a change in the relative positions of the dark/bright domains depending on the orientation of the polarizer axis with respect to the radial direction. However, in the TGB sample studied by us, the positions of the dark/bright bands remain unaltered upon sample rotation. Also this pattern is observed

even in the TGB$_A$ phase where there is no molecular tilt. So the existence of the radial structure in the TGB samples is due to an entirely different reason and could be attributed to distinct properties of the twist grain boundary liquid crystals. At the phase transition from TGB$_A$ to UTGB$_{C*}$ phase—compare region 3 in figures 2(*a*) and 2(*b*)—the radial structures retain similar features. The film thickness in this region is in the range of microns. The radial structures will be discussed in more detail in §3.2.

As the film thickness increases further and becomes comparable to the pitch of the TGB phase, the radial structures are replaced by the characteristic filaments of the TGB phase in the fourth region of the meniscus. The filaments usually extend concentrically parallel to the periphery of the hole. On rare occasions, they have been found to grow in different directions, including the radial one. By comparing parts (*a*) and (*b*) in figure 2, one notices the change of appearance of the filaments at the TGB$_A$ to UTGB$_{C*}$ phase transition with the appearance of undulations in the UTGB$_{C*}$ phase. The

film thickness in this region changes from microns to tens of microns. The detailed studies of the structures and properties of this part of the meniscus are given in §3.3.

In the meniscus region closest to the supporting wall, region 5, the film thickness is much larger than the pitch of the TGB structure for the studied mixture and can reach hundreds of microns at the supporting wall. The director patterns in this region of the meniscus are very complex, and will not be discussed in this paper.

3.2. *Radial structures*

Region 3, with the pattern of radial stripes, is the most interesting part of the meniscus, as such a structure had not been observed previously for TGB phases. Both FCPM and PM textures corresponding to the radial pattern have a relatively weak contrast compared with the structures in the thicker regions of the meniscus, such as the filaments. This indicates that deviations of the local director from the normal to the LC–air interface are small.

The average spatial periodicity of the radial stripes, λ_r, depends on the local thickness of the film. As seen in figures 2 and 5, λ_r increases with increase of thickness. There is no clear boundary between the second and third meniscus regions (figure 2). The contrast of the radial pattern is very weak in the thinner part of this region of the meniscus, and it is not very apparent whether the pattern becomes too small to be resolved by the optical microscope, or the radial structures exist only above some critical thickness.

The xy and xz FCPM sections with polarizer **P** along **x** (perpendicular to the thickness gradient) have rather
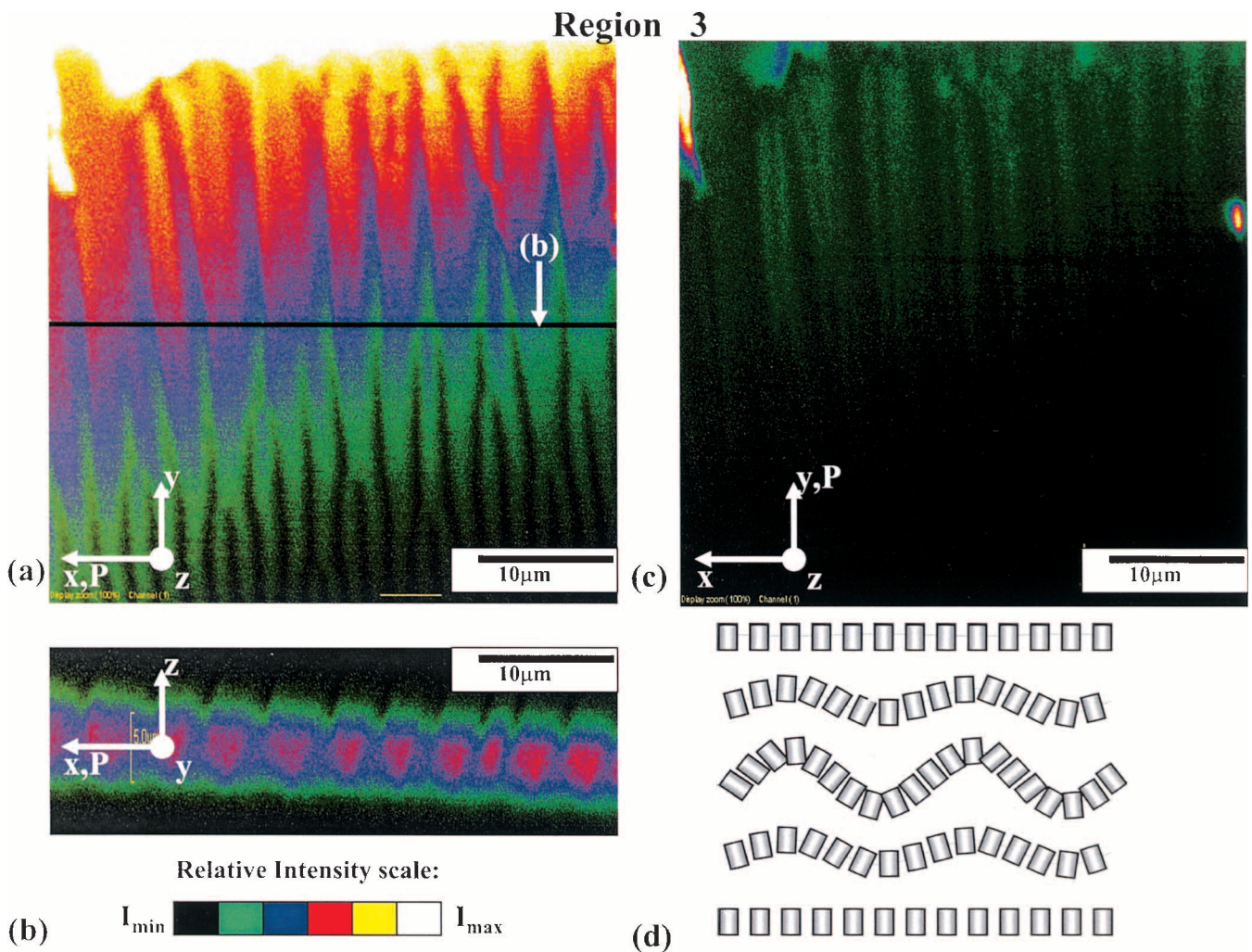
Figure 5. Radial structure in region 3: (*a*) and (*c*) FCPM textures from optical scans in the plane of the free-standing film for two orthogonal orientations of polarizer; (*b*) FCPM vertical cross-section along the black line in (*a*); (*d*) reconstructed director configuration for the vertical cross-section in (*b*).

strong fluorescent signals with good contrast. The FCPM signal for **P** along the thickness gradient (axis **y**) is much weaker, compare figures 5(c) and 5(a). Thus the local director $\hat{n}$ in the radial pattern is mostly in the xz plane, figure 5(d). The xz FCPM scans, figure 5(b), indicate a wave-like deformation and can be associated with layer undulations. The wavelength of these undulations increases toward the supporting wall. Detailed studies of the meniscus profile in the region of radial structures were carried out using experimental textures shown in figure 6. The fluorescent signal for the optical sections of region 2 and the thinner part of region 3 of the meniscus is rather weak, as the director is almost homeotropic in these regions. It is also sensitive to the reflections of the laser beam used for excitation. Thus, the optical fringes are also visible in

the xy optical sections, see figure 6(a). The relative change of the film thickness has been calculated, figure 6(d), using the fringes shown in figure 6(a). The FCPM vertical cross-sections of figures 6(b) and 6(c) are used to correlate the relative thickness measurements based on the fringes. The circular profile obtained as the best fit to the experimental data based on the fringes is extrapolated to the distances at which the xz vertical cross-sections (b) and (c) are taken, and the thickness is estimated taking into account the axial resolution. We also analyse the periodicity of the radial structures λ_r as a function of the distance Δy in the **y**-direction, figure 6(e). Interestingly, in the thinner part of the region with radial structures, λ_r increases stepwise, figures 6(a) and 6(e). This periodicity always remains unchanged along some
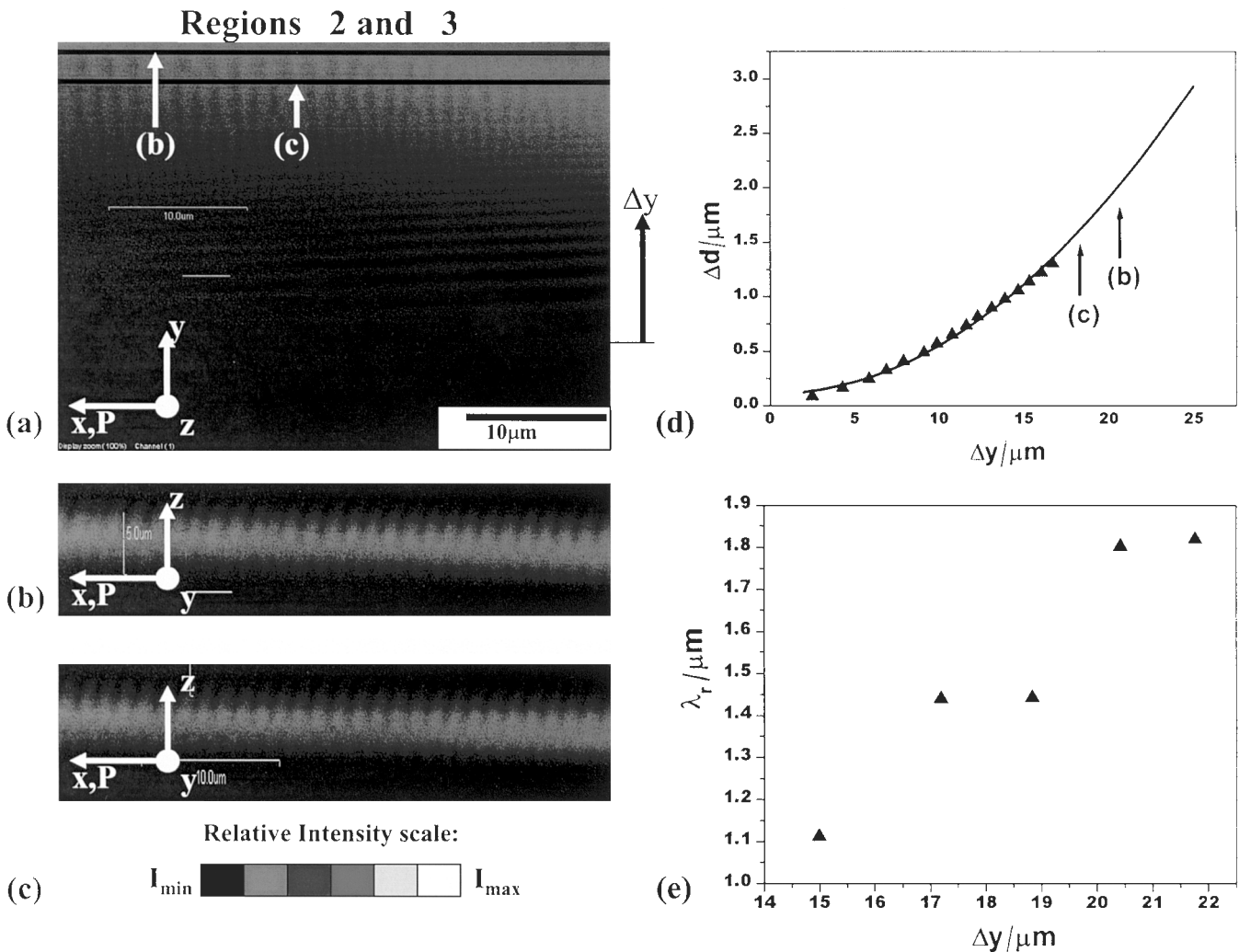
Figure 6. Pattern of the radial structure and interference fringes in region 3: (a) in-plane xy FCPM scan; (b) and (c) FCPM vertical cross-sections taken along the lines indicated in (a); (d) relative change of the film thickness Δd measured using the interference fringes versus the distance Δy; (e) spatial periodicity of the radial structure λ_r versus distance Δy. Solid line in (d) shows a circular fit to the experimental data; the arrows in (d) denote positions of the xz optical sections shown in (b) and (c).

distance in the **y** direction (parallel to the radial stripes) despite the thickness increase, and then the periodicity jumps to a larger value, figure 6 (*a*). The lines along **x**, at which the radial structures experience the sudden changes of the spatial periodicity λ_r may correspond to the location of the dislocations of large Burger's vectors.

The model of the director field that satisfies these experimental observations is shown in figure 7. The inset of figure 7 shows the FCPM vertical cross-section in the plane normal to the radial pattern, with the polarizer also in the plane of the section. According to the model, the director deviations from the homeotropic orientation are normal to the radial stripes. A possible origin of this pattern is the following. The thickness increase is relaxed by insertion of additional layers in the bulk of the film and by formation of dislocations of large Burger's vectors, which are separated by rather large distances. Evidence for edge

dislocations with large Burger's vectors, has also been previously seen in lyotropic slabs of large thickness [23]. The strong surface tension at the LC–air interface (about $30 \, \text{dyn} \, \text{cm}^{-1}$ [12]) requires a smooth surface profile of the film, and thus leads to regions of a large tensile (dilative) strain. It has been shown [24] that when the tensile strain exceeds a value $\approx 2\pi \lambda_1 / l_{sm}$ the layers can undulate to fill space. Here $\lambda_1 = \sqrt{K_{11}/B}$ is the splay penetration length, and l_{sm} is the smectic layer spacing. The director field in the vertical section of film, reconstructed from the FCPM xz scan, figure 5 (*d*), is in agreement with the director deformations of undulation type. As the film thickness increases, the spatial periodicity (wavelength) of undulations, λ_r, also increases, as clearly seen from PM (figure 2) and FCPM (figures 5 and 6).

The sinusoidal undulations depicted in figures 5 (*d*) and 7 represent an idealized model of the radial structure. Experimental data, figure 5 (*c*), suggest that
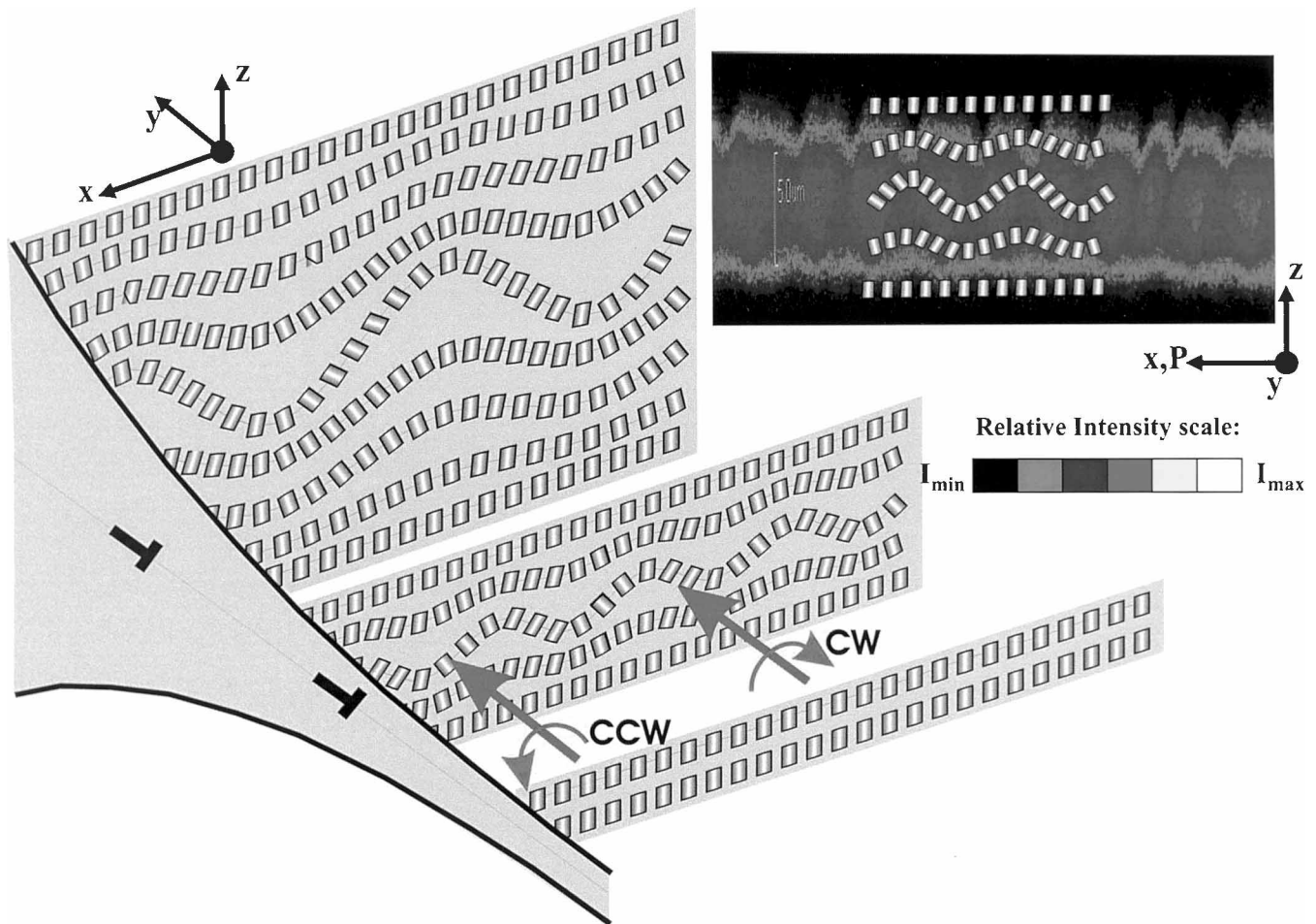
Figure 7. Schematic representation of the director structures in the region with the radial pattern and edge dislocations of large Burger's vectors (region 3 in figure 2). Undulation of the layers takes place in regions with tensile strain. The insert shows the director pattern on top of an experimental FCPM texture of the vertical cross-section of the film.

the undulations are less symmetric: two adjacent shoulders of the undulation wave are of different length. Similar asymmetric undulations have been observed in lyotropic 'rippled' phases [25], undulating chevron tips of chiral SmC* liquid crystals [26] and near the substrates of a cell filled with undulating cholesteric liquid crystals [27]. The asymmetry can be caused by different reasons, including finite anchoring at the interface [27] and the chiral nature of the material. The latter mechanism has been discussed for lyotropic phases in [28]. In the present situation, asymmetry can be caused by coupling between two types of twist: twist caused by thickness gradients in the film and twist caused by molecular chirality, as discussed below.

When one moves from region 2 where the normal to the layers is vertical, to region 3, where it is tilted by undulations, one observes a twist of the normal to the layers. The two adjacent shoulders of the undulation wave are associated with different handedness of the twist, clockwise and counterclockwise, see the left part of figure 7. In a non-chiral material, the two modes would be of the same energy. However, in the chiral

material we are dealing with, the intrinsic twist facilitates one twist mode and hinders the other. Therefore, the coupling between the twist imposed on the undulation pattern by the thickness gradient and the twist originating in the intrinsic molecular chirality, might lead to the observed asymmetry of undulating patterns.

3.3. *TGB filaments*

Filaments characteristic of the TGB_A phase can be observed in the fourth region of the meniscus. Similar director structures are known from the literature, and could be obtained in confined TGB_A samples [29]. The film thickness in the region exhibiting filaments is larger than the TGB pitch, and the helical structure is not suppressed by the homeotropic boundary conditions imposed at the LC–air interface. The PM texture of the filaments has the appearance of periodic stripes parallel to the periphery of the hole, figure 2(a). When the sample is cooled into the $UTGB_{C*}$ phase, the filaments undulate, as has been observed previously [9], figure 2(b). The FCPM texture of this region of meniscus also has
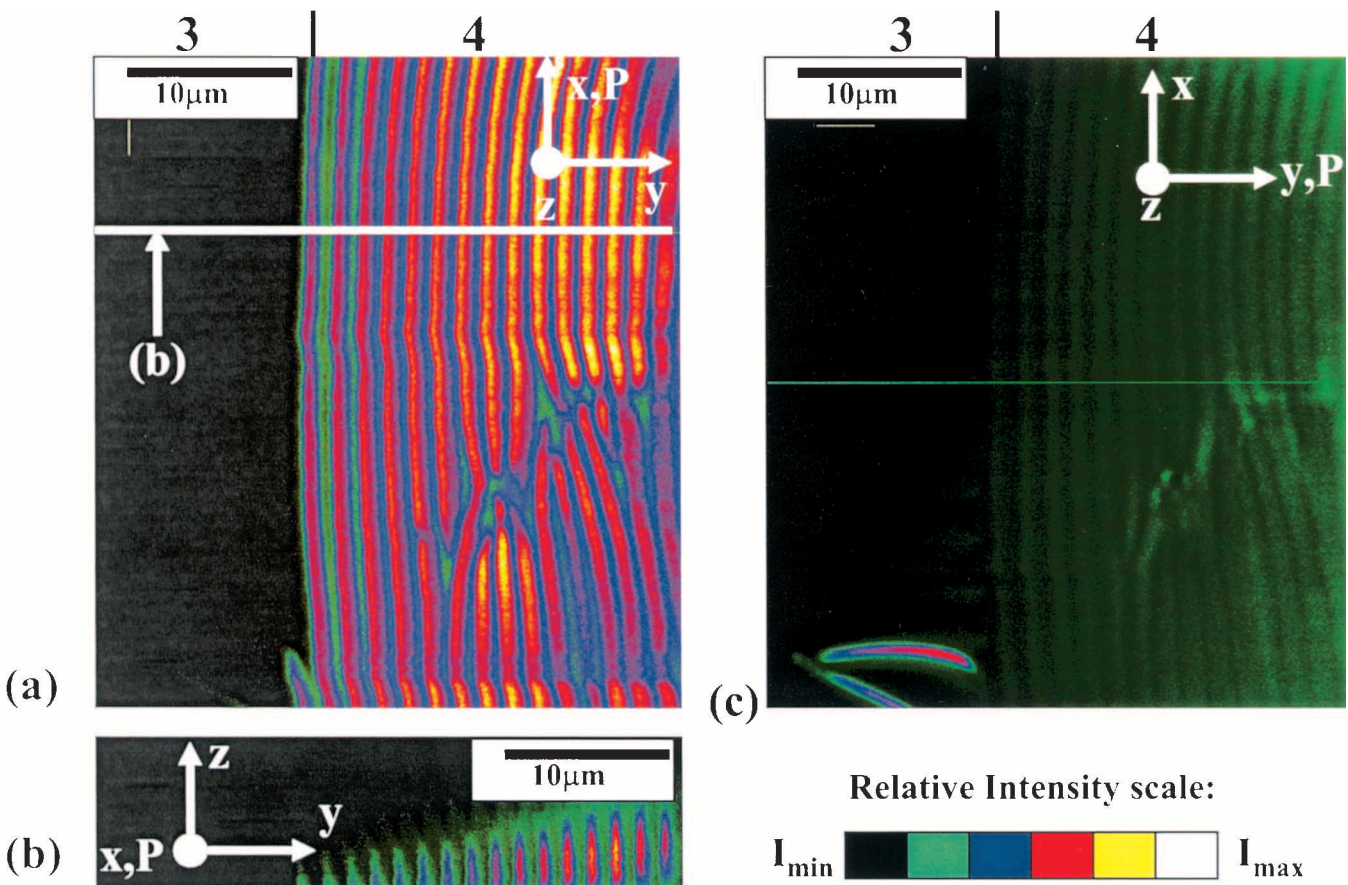
Figure 8. FCPM textures of filaments of the TGB_A phase (region 4): (a) and (c) xy optical sections for two orthogonal orientations of the polarizer; (b) FCPM vertical cross-section along the line shown in (a).
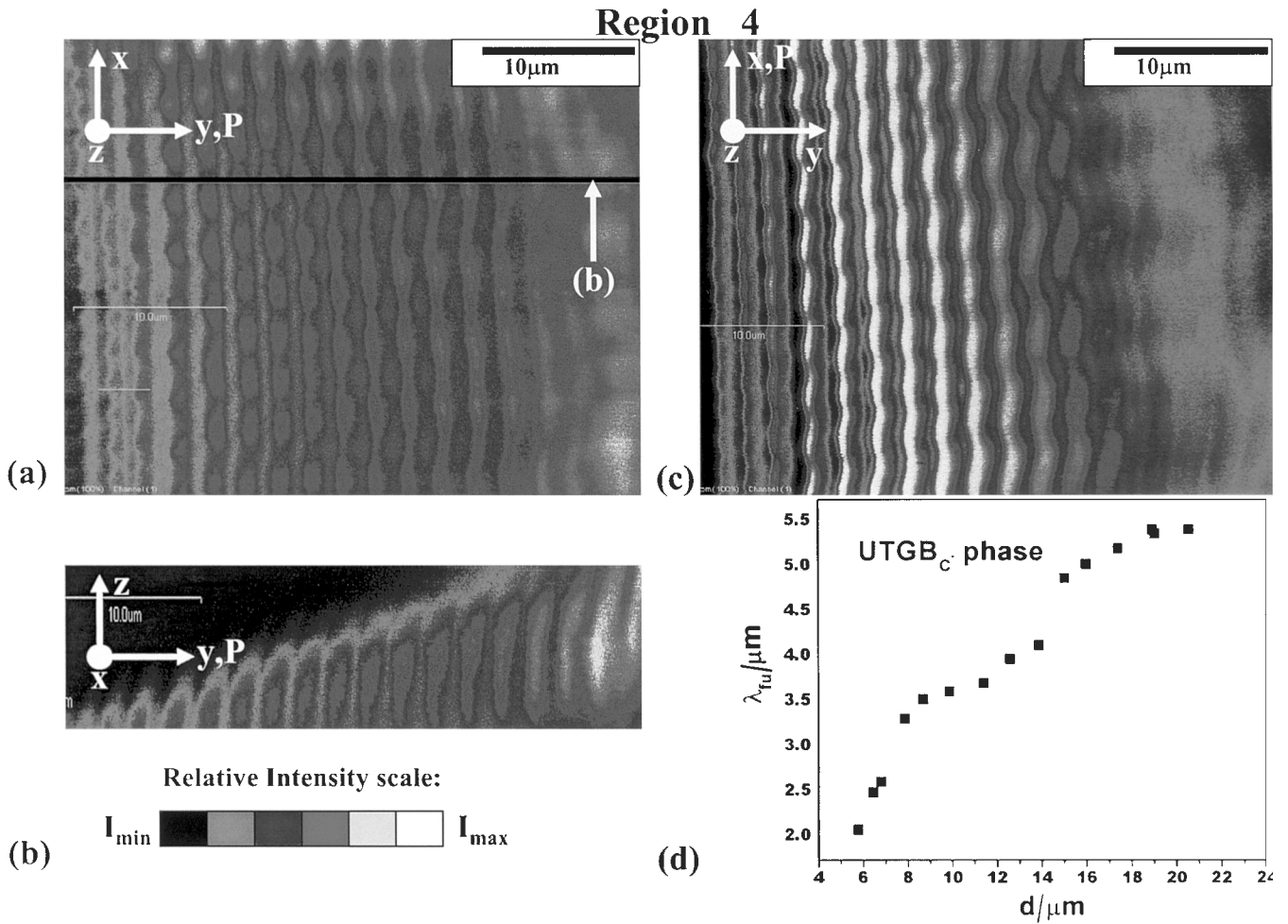
Region 4

Figure 9. FCPM textures of filaments in the UTGB$_{C*}$ phase in the same sample as shown in figure 8 (region 4): (*a*) and (*c*) *xy* optical sections for two orthogonal orientations of the polarizer; (*b*) FCPM vertical cross-section along the line shown in (*a*); (*d*) variation of the undulation wavelength of the filaments, λ_{fu}, with the film thickness.

the appearance of periodic stripes, figures 8, 9. Most often, the filaments are found to be normal to the thickness gradient in the meniscus. However, they can also grow along the radial direction and at some angles to it; often the filaments grow discontinuously, figure 8. The fluorescence signal for the FCPM scans with polarizer along the length of the filaments is consistent with the periodic stripes of strong and weak signal figure 8 (*a*), whereas the signal is comparatively weak for the scan with polarizer along the thickness gradient, i.e. the *y* axis. The situation is completely reversed for the filament that grows in the radial direction, figures 8 (*a*) and 8 (*c*). The FCPM scans prove the basic model of TGB filaments in which each filament corresponds to a rotation of the director by π radians. The width of the filament is comparable to half the pitch of the TGB helix. The local director in the structure of the filament is mainly in the plane parallel

to the filament. The vertical *yz* section in figure 8 (*b*) showing the top part of the film (from the film mid-plane to the top LC–air interface) allows for a rough estimate of thickness in this region of the meniscus. Since the defocusing effects limit the depth of FCPM scanning (which becomes smaller than the film thickness in this region of meniscus), a better estimate of the film thickness in this region is difficult.

The UTGB$_{C*}$ filaments exhibit strong undulations, figures 2 (*b*) and 9. Unlike the TGB$_A$ filaments, the UTGB$_{C*}$ filaments give a strong fluorescence signal in FCPM textures with both orthogonal orientations of polarizer, figures 9 (*a*) and 9 (*c*). This shows that in the UTGB$_{C*}$ phase the local director field in the filaments has components in all three directions, **x**, **y**, and **z**. The vertical FCPM section, figure 9 (*b*), was used for thickness estimates. Interestingly, the wavelength of the undulations of the filaments λ_{fu}, increases with

increase of the film thickness, figure 9. The general trend of this dependence is to saturate at some value, that corresponds to the undulation wavelength for unbounded LC in the UTGB$_{C*}$ phase.

4. Conclusions

The meniscus of free-standing films of TGB liquid crystals has been investigated using FCPM. We describe five distinct regions of the meniscus with different director structures and defects, some of which are common for meniscus regions of other lamellar systems, and others that are unique for the TGB phases studied.

In particular, we have found a periodic radial pattern in the intermediate thickness region of the meniscus, which is specific only to the TGB phases. We attribute this pattern to layer undulations of the unwound smectic layers in the freely suspended film. The undulation-type deformations result from the large tensile (dilative) strain occurring between dislocations of large Burger's vectors.

The FCPM studies reveal that when the film thickness is larger than the TGB pitch, filamentary texture is observed. The 3D director pattern of the filaments is similar to the ground state director fields of TGB$_A$ and UTGB$_{C*}$ liquid crystals. The characteristic wavelength of undulation of the UTGB$_{C*}$ filaments increases with the film thickness and shows a trend to saturate when the film thickness is much larger than the TGB pitch.

References

[1] DE GENNES, P. G., 1972, *Solid State Commun.*, **10,** 753.
[2] RENN, S. R., and LUBENSKY, T. C., 1988, *Phys. Rev. A*, **38,** 2132.
[3] GOODBY, J. W., WAUGH, M. A., STEIN, S. M., CHIN, E., PINDAK, R., and PATEL, J. S., 1989, *Nature*, **337,** 449.
[4] LAVRENTOVICH, O. D., NASTISHIN, YU. A., KULISHOV, V. I., NARKEVICH, YU. S., TOLOCHKO, A. S., and SHIYANOVSKII, S. V., 1990, *Europhys. Lett.*, **13,** 313.
[5] IHN, K. J., ZASADZINSKI, J. A. N., PINDAK, R., SLANEY, A. J., and GOODBY, J. W., 1992, *Science*, **258,** 275.
[6] RENN, S. R., and LUBENSKY, T. C., 1991, *Mol. Cryst. liq. Cryst.*, **209,** 349.
[7] RENN, S. R., 1992, *Phys. Rev. A*, **45,** 953.
[8] NAVAILLES, L., PINDAK, R., BAROIS, P., and NGUYEN, H. T., 1995, *Phys. Rev. Lett.*, **74,** 4245.
[9] PRAMOD, P. A., PRATIBHA, R., and MADHUSUDANA, N. V., 1997, *Curr. Sci.*, **73,** 761.
[10] PRAMOD, P. A., HATWALNE, Y., and MADHUSUDANA, N. V., 2001, *Liq. Cryst.*, **28,** 525.
[11] SONIN, A. A., 1993, *Freely Suspended Liquid Crystalline Films* (John Wiley).
[12] GEMINARD, J. C., HOŁTVSYST, R., and OSWALD, P., 1997, *Phys. Rev. Lett.*, **78,** 1924.
[13] PICANO, F., HOŁYST, R., and OSWALD, P., 2000, *Phys. Rev. E.*, **62,** 3747.
[14] NASTISHIN, YU. A., KLEMAN, M., MALTHETE, J., and NGUYEN, H. T., 2001, *Eur. Phys. J. E.*, **5,** 353.
[15] KLEMAN, M., NASTISHIN, YU. A., and MALTHETE, J., 2002, *Eur. Phys. J. E.*, **8,** 67.
[16] DHARA, S., PRATIBHA, R., and MADHUSUDANA, N. V., 2002, *Ferroelectrics*, **277,** 13.
[17] SMALYUKH, I. I., SHIYANOVSKII, S. V., and LAVRENTOVICH, O. D., 2001, *Chem. Phys. Lett.*, **336,** 88.
[18] SHIYANOVSKII, S. V., SMALYUKH, I. I., and LAVRENTOVICH, O. D., 2001, in *Defects in Liquid Crystals: Computer Simulations, Theory and Experiments*, edited by O. D. Lavrentovich, P. Pasini, G. Zannoni, and S. Žumer, NATO Science Series. (Kluwer Academic Publishers).
[19] MADHUSUDANA, N. V., MOODITHAYA, K. P. L., and SURESH, K. A., 1983, *Mol. Cryst, Liq. Cryst.*, **99,** 239.
[20] LEICEK, L., and OSWALD, P., 1991, *J. Phys. II Fr.*, **1,** 931; PERSHAN, P. S., 1974, *J. Appl. Phys.*, **45,** 1590.
[21] SMALYUKH, I. I., and LAVRENTOVICH, O. D., 2003, *Phys. Rev. Let.*, **90,** 085503; SMALYUKH, I. I., and LAVRENTOVICH, O. D., 2002, *Phys. Rev. E.*, **66,** 051703.
[22] MEYER, R. B., and PERSHAN, P. S., 1973, *Solid State Commun.*, **13,** 989.
[23] NALLET, F., and PROST, J., 1987, *Europhys. Lett.*, **4,** 307.
[24] DE GENNES, P. G., and PROST, J., 1993, *The Physics of Liquid Crystals* (Oxford Science Publications).
[25] WACK, D. C., and WEBB, W. W., 1988, *Phys. Rev. Lett.*, **61,** 1210.
[26] SUBACIUS, S. D., VOLOSCHENKO, D., BOS, P., and LAVRENTOVICH, O. D., 1999, *Liq. Cryst.*, **26,** 295.
[27] ISHIKAWA, T., and LAVRENTOVICH, O. D., 2001, *Phys. Rev. E.*, **63,** 030501.
[28] CHEN, C.-M., LUBENSKY, T. C., and MACKINTOSH, F. C., 1995, *Phy. Rev. E.*, **51,** 504.
[29] DIERKING, I., and LAGERWALL, T., 1999, *Liq. Cryst.*, **26,** 83.